Optical properties in waters around the Mendeleev Ridge related to the physical features of water masses

Jinping Zhao [a], Weibo Wang [a], Sung-Ho Kang [b], Eun-Jin Yang [b], Tae-Wan Kim [b]

[a] Physical Oceanography Lab, Ocean University of China
[b] Korea Polar Research Institute

ARTICLE INFO

ABSTRACT

Irradiance profiles were measured during the Korean 2012 summer Arctic Ocean cruise and optical properties were studied. The optical attenuation coefficient in all surface waters was low, as the nutrients in the surface layers became exhausted and phytoplankton growth was only possible at the subsurface where optimal conditions of nutrients and sufficient illumination existed. This high attenuation zone was at about 40–60 m. The attenuation properties were categorized to three types. Type-1 waters had weaker maximum attenuation coefficients and were located at the Chukchi Plateau and the north margin of the study region. Type-2 water had an intense maximum of attenuation coefficient up to 0.56/m located on west flank of Mendeleev Ridge and continental slope of East Siberian Sea. Two integral parameters, attenuation depth and optical thickness, were mapped by spatial distribution. The attenuation depth was basically shallower (40 m) to the west and deeper to the east (100 m). The averaged optical thickness at the level of 30–60 m was the main zone of high attenuation. Both the optical attenuation property and the physical features of the water indicated two subsurface water masses: one is the cold shelf water well mixed with river water and transported to the east by a subsurface current along the East Siberian Slope. The other is the warmer water from the Pacific with lower nutrients and transported to the northwest along the north margin of the observed region. A cyclonically re-circulated branch of shelf water passing over the Chukchi Abyssal Plain was described in this study.

© 2015 Elsevier Ltd. All rights reserved.

1. Introduction

The absorption capacity of seawater to solar radiation is important to oceanic thermal structure (Chang and Dickey, 2004). As solar radiation entering into the ocean is mainly in visible wavebands, optical observation is important for solar energy absorption in seawater.

In the Arctic, sea ice is a major factor influencing solar radiation penetration into the ocean. More than 80% of solar radiation is reflected back to space from the surface of snow and ice, but less than nine percent of the solar radiation energy arriving to open water is similarly reflected. Over the past few decades Arctic seasonal sea ice has decreased in extent and concentration (Tucker et al., 2001; Lindsay and Zhang, 2005). The summer extent of the Arctic sea ice cover reached a minimum in September 2007 (Stroeve et al., 2008; Perovich and Richter-Menge, 2009), followed by a new minimum record on September 19, 2012 [http://nsidc. org/arcticseaicenews/2012/09/arctic-sea-ice-extent-settles-at-re cord-seasonal-minimum/]. Reduced internal ice stress allows a more efficient coupling of wind forcing to the upper ocean, and increases the flux of warm Pacific Summer Water (Shimada et al., 2001; Steele et al., 2004) into the basin and caused the cata-strophic changes of sea ice (Shimada et al., 2006). Sea ice retreat influences the Arctic atmosphere-ice-ocean system (Perovich et al., 2007). An increase in open water has an accelerating effect on ice–albedo feedback and sea ice retreat (Perovich et al., 2008).

The propagation of light in the ocean is influenced not only by the molecular structure of seawater, but also by colored dissolved organic matters (CDOM), suspended detritus and phytoplankton. These substances influence the propagation and attenuation of sunlight with depth. In the Canada Basin, the distribution of CDOM is relatively uniform and its influence on optical property is easy to recognize (Wozniak and Dera, 2007). The influence of the detritus is most important in the blue and red wavelengths, which can be conveniently determined from multi-spectral instrument mea-surements. Phytoplankton in seawater also absorbs solar radiation for photosynthesis, so the depths of the maximum chlorophyll-a and the maximum attenuation coefficient typically coincide (Manizza et al., 2005).

E-mail addresses: jpzhao@ouc.edu.cn (J. Zhao),
bobobufei@ouc.edu.cn (W. Wang), shkang@kopri.re.kr (S.-H. Kang),
ejyang@kopri.re.kr (E.-J. Yang), twkim@kopri.re.kr (T.-W. Kim).

The radiance, irradiance, and the derived diffuse attenuation coefficients are the apparent optical properties (AOP), which describe the more realistic radiative conditions in the water. In the polar region, light enters the ocean through leads or the partly ice free surface, and the adjacent sea ice adds it own impacts to AOP. Dickey et al. (2006) demonstrated that the diffuse attenuation coefficients are quasi-inherent optical properties since they often depend only weakly on the ambient light field. Close relationships often exist between the vertical diffuse attenuation coefficient $K_d(\lambda)$ and the absorption coefficient $a(\lambda)$. $K_d(\lambda)$ can be separated into four types of contributions due to the various constituents (e.g., water, phytoplankton, detritus, and CDOM) in analogy to the absorption coefficients (see Morel, 1988; Gordon, 1991; Morel and Maritorena, 2001).

The Korean 2012 summer cruise studied a quasi-rectangular region between 170°E-150°W, 75–79°N, including the Mendeleev Ridge, the Chukchi Abyssal Plain, the Chukchi Cap, and the Northwind Ridge (Fig. 1). Woodgate et al. (2007) labeled this area as the Mendeleev Ridge and Chukchi Borderland (CBLMR) region. The cruise from August 4 to September 6 of 2012 was organized by the Korea Polar Research Institute (KOPRI) and used the Korean icebreaker ARAON. The water sources of upper ocean in the observed area are complex. This part of Canada Basin is dominated by Pacific Water, whereas in the Makarov Basin, just west of the study area, it is dominated by Atlantic source water (Jones et al., 1998). In the observed area the surface waters from Pacific and Atlantic meet together. Below the halocline, Atlantic waters are carried by a topographically-steered boundary current (Woodgate et al., 2007). Atlantic Water of the lower halocline is upwelled onto the Chukchi Sea slope/shelf to mix diapycnally with less dense Pacific Water (Woodgate et al., 2005). This enhanced shelf break upwelling can be expected to increase the availability of nutrients to the shallower shelves (ACIA, 2005).

Runoff into the East Siberian Sea discharges materials that includes suspended matter and nutrients (Gordeev et al., 1996; Wegner et al., 2003). The total suspended matter exported from the Russian territory is 102×10^6 t/year, and 25.15×10^6 t/year of total enters the East Siberian Sea (Gordeev, 2006). Freshwater affects stratification in much of the Arctic Ocean (Schlosser et al., 2002), with runoff transported in the Transpolar Drift over a time scale of about three years (Jahn et al., 2010). Advection of inflows from marginal shelves and seas (Gordeev, 2006), as well as rivers import nutrients to support phytoplankton growth (Matsuoka et al., 2009).

Ice-free continental shelves often experience intense seasonal blooms of phytoplankton owing to favorable nutrient and light conditions (Hill and Cota, 2005). Ice edge blooms are a conspicuous feature in the seasonal cycle of Arctic ecosystems with the high production in the East Siberian Sea (Perrette et al., 2011). These occur when water, rich in nutrients, is first exposed to sunlight during springtime sea-ice melt (Popova et al., 2010). Enhanced solar radiation into the ocean through leads or waters in the marginal ice zone (MIZ) enables photosynthesis in icy water. However, sea ice shades most sunlight from entering into the ocean and lowers the illumination of the underlying ocean, which limits phytoplankton growth although some seasonal conditions benefit phytoplankton growth in the summer. Since 1998, open water area in the Arctic has increased at the rate of 0.07×10^6 km^2 a^{-1}, with the greatest increases in Siberian sectors, which lead to higher rates of annual production (Pabi et al., 2008).

Annual primary production is generally controlled by nutrient availability, so the surface concentrations of nitrate, phosphate and silicic acid in Arctic waters approach detection limits after the spring bloom (Sakshaug, 2003). The nutrients supplied by Pacific Winter Water combined with light penetration without sea ice cover could produce a prominent chlorophyll *a* maximum layer (Nishino et al., 2008).
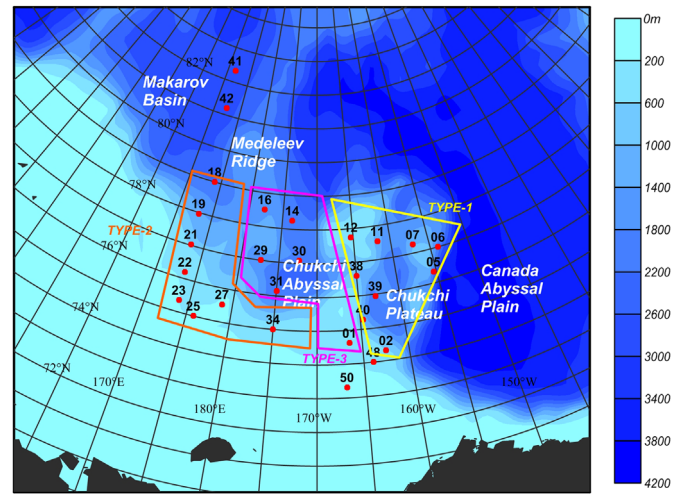

Fig. 1. Locations of stations with available irradiance data (red points). Areas with similar optical types are delineated by colored polygons. (For interpretation of the references to color in this figure legend, the reader is referred to the web version of this article.)

Biophysical effects are an important interaction between physical and ecological processes in the upper ocean (Dickey, 1991; Sathyendranath et al., 1991; Siegel et al., 1995). Phytoplankton absorb solar energy via pigments and thereby modify upper ocean temperature (Morel, 1988; Strutton and Chavez, 2004). The increased water temperature speeds up ice melting and changes the temperature profile of the upper ocean. It is reported that in high latitude regions, the surface temperature warms by 0.1–1.5 °C in spring/summer as a result of this absorption (Manizza et al., 2005). The presence of phytoplankton also reduces the vertical penetration of heat and cools subsurface water (Nakamoto et al., 2000). The altering of the water optical properties may change the density field of the ocean and the dynamical response of the oceanic layers to surface wind stress forcing (Shell et al., 2003). Therefore, spatial distribution of optical properties is usually taken into account in ocean numerical models (Jerlov, 1976).

In the Arctic, the optical properties of seawater are not only related to biological processes, but also to physical oceanographic water masses. Previous studies suggested that bio-optical properties in polar waters are markedly different from lower-latitude ecosystems with highly packaged cells and lower chlorophyll-specific absorption (Mitchell and Holm-Hansen, 1991; Mitchell, 1992; Sathyendranath et al., 2001). The absorption of light by phytoplankton is also species and size dependent (Yentsch and Phinney, 1989).

Measurements for optical properties in the Arctic Ocean are still rare (e.g. Mitchell, 1992; Pegau, 2002). In this study, data on irradiance, chlorophyll-a, and nutrients collected during the Korean 2012 summer cruise are used to describe the attenuation features of incident solar radiation.

2. Measurement instruments, data, and method

A high-resolution optical profiling system was used to measure irradiance and radiance in the upper water column (Model PRR-800, Biospherical Inc. San Diego, USA). The instrument includes a separate unit, Model PRR-810, measuring downwelling irradiance from the sea surface. This PRR system is configured to measure at 18 wavebands: 313, 380, 412, 443, 490, 510, 520, 532, 555, 565, 589, 625, 665, 683, 710, 765, 780 and 875 nm with 10 nm bandwidth. A compact-CTD (ALEC Inc., Kobe, Japan) was deployed together with PRR-800, and is equipped with temperature,

salinity, pressure, fluorescence and turbidity sensors. Chlorophyll-a concentrations (hereafter referred as chlorophyll) were determined from the fluorescence data.

The combined PRR/MCTD system was deployed to maximum depths of 125 m at all daytime stations and 27 profiles in total were obtained (Fig. 1). Quality assurance assessments resulted in some measurements being excluded for following reasons: measurements in insufficiently light conditions; measurements in depths of less than 50 m; data strongly influenced by sun glitter; accidental shading of the surface unit by ship superstructure, etc.

The two northernmost stations were ice covered. With the exception of these two stations, all other profiles were obtained in ice-free water, though sea ice was present at some stations. The optical instrument was kept at a distance of tens of meters from sea ice. Because of these precautions, we neglected any possible impacts of ice shading on the instrumental measurements.

Downwellng irradiance, E_d, in seawater is described by (Mueller and Fargion, 2003)

$$E_d(z,\lambda) = E_d(0^-, \lambda) \exp\left[-\int_0^z k_d(z',\lambda)dz'\right] \tag{1}$$

or alternately by

$$-\int_0^z k_d(z',\lambda)dz' = \ln[E_d(z,\lambda)] - \ln[E_d(0^-,\lambda)] \tag{2}$$

where z is the vertical coordinate, 0^- is at just under sea surface, and $k_d(z,\lambda)$ is the attenuation coefficient of irradiance. Standard analysis is to estimate $k_d(z,\lambda)$ as the local slope of $\ln[E_d(z,\lambda)]$ (Smith and Baker, 1984, 1986),#i.e. $k_d(z,\lambda)$is a wavelength-dependent constant within $\pm\Delta z$ of the median depth z_m ($z_m - \Delta z \le z \le z_m + \Delta z$), and

$$\ln[E_d(z,\lambda)] = \ln[E_d(z_m,\lambda)] - (z-z_m)k_{dm}(\lambda) \tag{3}$$

where the intercept $\ln[E_d(z_m,\lambda)]$ and the slope $k_{dm}(\lambda)$ are unknown and determined by the least squares method. The choice for the half-width Δz is somewhat arbitrary. Smith and Baker (1984, 1986) recommended Δz as 4 m in deep ocean waters and greater depths in coastal waters to limit instrumental noise.

3. Optical attenuation properties and types

Physical features and the optical properties of water masses are often independent parameters. For example, the physical characteristics of a water mass are determined by temperature and salinity, whereas optical properties are determined by water molecules, algal, CDOM, and particulate debris. Often optical properties are consistent with the physical features of water masses, because in a well-mixed water mass, the spatial distribution of a particulate substance is uniform. However, in some situations, there can be different optical properties even in the same water mass, because of different illumination conditions, such as in ice covered waters.

The optical attenuation coefficient reflects not only information on distributions of particulate and dissolved substances in a water mass, but also regional differences in phytoplankton growth under different nutrient concentrations and illumination conditions (Hill and Cota, 2005). The optical attenuation coefficient is usually highly correlated with chlorophyll concentrations (Manizza et al., 2005). The maximum optical attenuation coefficient at 490 nm versus the chlorophyll concentration at the same depth of each station are plotted in Fig. 2. The low attenuation coefficients clustered at 0.06–0.08/m, a little bit higher than 0.018/m of the pure seawater absorption coefficient without algae.

High chlorophyll concentrations were identified by attenuation coefficients higher than 0.1/m at 10 of 20 stations. Very high
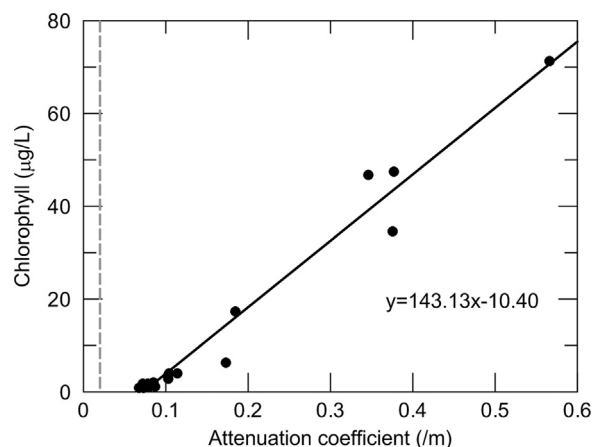

Fig. 2. Correlation of the maximum optical attenuation coefficient of 490 nm and the chlorophyll concentration at the same depth. The solid line is the best-fit regresssion with the correlation coefficient of 0.985. The lowest maximum optical attenuation coefficient is about 0.06–0.08/m. As a reference, the attenuation by pure seawater without algae is 0.018/m as shown by the dashed line.

attenuations were up to 0.37/m and the maximum was 0.566/m. The solid line (Fig. 2) is the best-fit regression with the correlation coefficient of 0.985. We concluded therefore, that in the observed region, the optical attenuation coefficients are controlled by algal concentrations.

3.1. Types of attenuation profiles

Seawater has the highest transparency at the 490 nm waveband among all spectra of solar radiation. We used the attenuation coefficient at 490 nm as a basis to identify the different attenuation properties.

The water far from the shelf, including Stations 41 and 42 was covered by sea ice. A high attenuation coefficient of more than 0.14/m was observed in the surface 20 m of the water column. This indicates sufficient nutrients for phytoplankton reproduction at the surface (Jiang et al., 2015). An attenuation coefficient of about 0.06/m, close to the minimum in the clear sea water was observed in the subsurface. Another special water is typical shelf water (Station 50) with a vertically uniform intense attenuation coefficient, more than 0.1/m. With the exclusion of these three stations, three characteristic types of attenuation were identified (Fig. 3) across the study region (Fig. 1).

Most stations with Type-2 waters were located over the west flank of Mendeleev Ridge and continental slope area, including stations 18, 19, 21, 22, 23, 25, 27, and 34. Type-2 waters had an intense attenuation coefficient at about 30–45 m. The maximum attenuation coefficient of 0.56/m appeared at Station 22. The surface waters in this area in spring might be nutrient-rich. We speculate that the nutrients were river-origin and supported an intense phytoplankton bloom following sea ice melt. The surface level nutrients became exhausted at the moment of the observation, so the biomass with chlorophyll maximum sank deeper to utilize available nutrients. As examples, the representative nutrient profiles (colloidal silicon dioxide, SiO_2) associated with Type 1, 2, and 3 waters (Stations 06, 19, 30) are shown in Fig. 4. SiO_2 concentrations were very low above the optical attenuation maximum at all stations, but reached high levels under the attenuation maximum. In the high-attenuation slope (Type 2) waters, the maximum SiO_2 concentration appeared at about 100 m, while in low-attenuation Pacific-origin (Type 1 and Type 3) waters, the SiO_2 maximum occurred below 150 m.
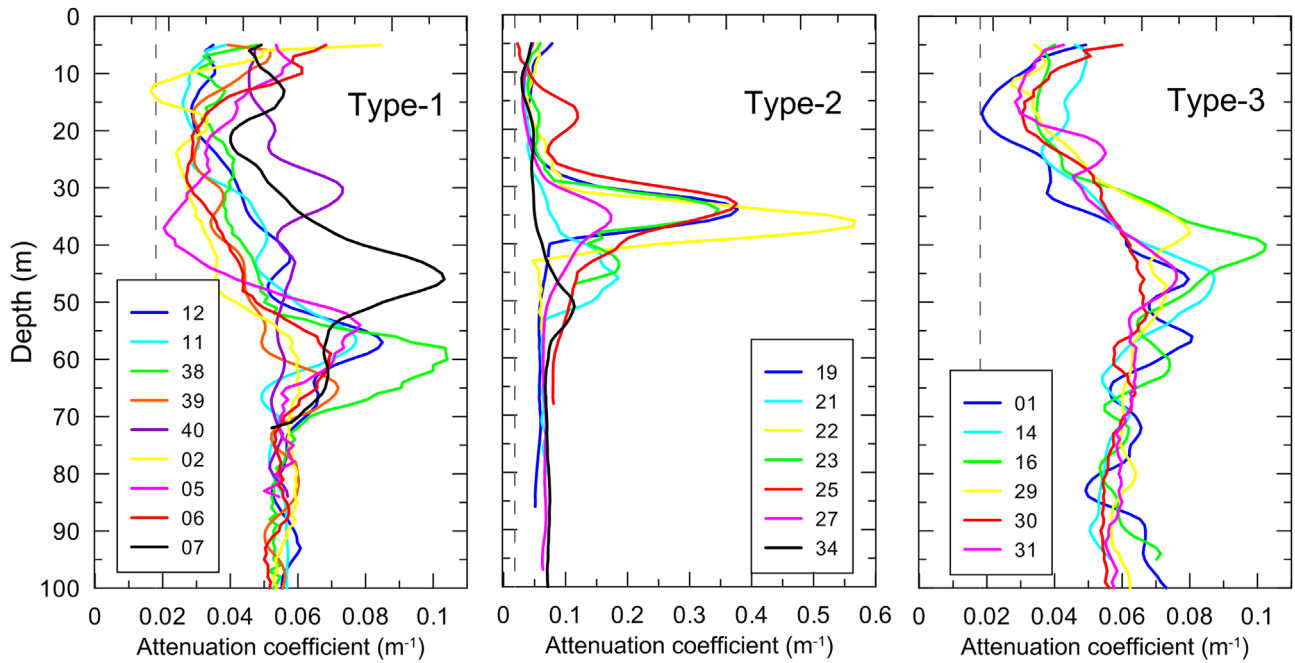
Fig. 3. Three identified types of optical attenuation properties observed at 490 nm.
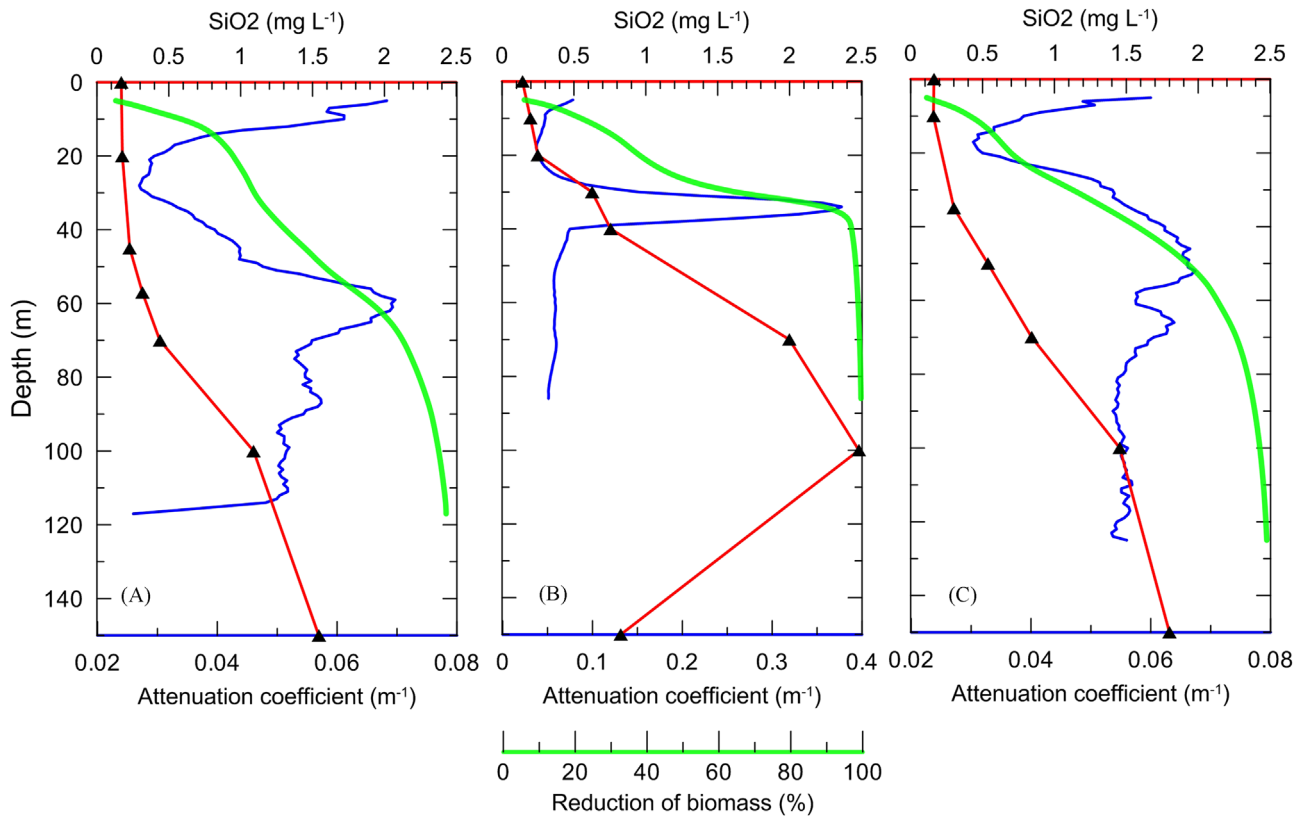

Fig. 4. Profiles of attenuation coefficients and nutrients. (a), (b), and (c) are profiles of representative stations (06, 19, 30) for Types 1, 2, and 3 water. Red lines are the profile of colloidal silicon dioxide (SiO₂). Blue lines are the attenuation coefficient of 490 nm. Green lines are the reduction rate related to biomass. (For interpretation of the references to color in this figure legend, the reader is referred to the web version of this article.)

Here we define a function η, the reduction rate, to reflect the optical attenuation by biomass,

$$\eta(z) = \left\{ 1 - \frac{\exp\left[-\int_0^z k_d(z',\lambda)dz'\right]}{\exp\left[-\int_0^z k_{d0}(z',\lambda)dz'\right]} \right\} \times 100 \qquad (4)$$

where k_d and k_{d0} are attenuation coefficients of measured and pure seawater, respectively. If there is no biomass, the reduction rate should be 0, while it should be 100 if the light is totally shaded. Light at 490 nm was used to calculate the reduction rate. In the slope water (Type-2, Station 19, Fig. 4b), the light was weakly attenuated in the upper ocean, but with nearly 100%

reduction (green line in Fig. 4b) at the maximum of attenuation coefficient (consistent with the maximum chlorophyll concentration). The high reduction rate resulted in a dark environment below ~ 40 m limiting primary production and associated uptake of SiO_2. Whereas in the Pacific origin water (Type-1, Station 06, Fig. 4a), there was still some light under the attenuation maximum, the nutrient was consuming there, and the nutrient maximum (much lower than that in Type -2 water) appeared in deep part where the light was totally reduced. The nutrient profile in Type-3 water (Fig. 4c) was similar with Type-1 water, but the concentration of SiO_2 was higher, showing a result of mixing with Type-2 water.

Type-1 water was similar to Type-2, but with a weaker maximum attenuation coefficient, less than 0.1/m (Fig. 3a). The stations within Type-1 area were all located at the Chukchi Plateau and the north margin of the observed region, including Stations 02, 05, 06, 07, 11, 12, 38, 39, and 40. The variation of algae in Type-1 area was similar to Type-2, but the much weaker chlorophyll maximum indicates lower nutrient concentrations in spring.

The maximum attenuation coefficient of Type-3 water was very weak, less than 0.08/m, which was nearly the same magnitude as underlying waters. The stations with Type-3 water were distributed in the center of the Chukchi Abyssal Plain. Weak attenuation was associated with low concentrations of chlorophyll, suggesting recirculated oligotrophic waters, with low phytoplankton production cropped by zooplankton.

The optical properties suggest that there were two water masses in the observed region. One was shelf water with the optical features of Type-2, which was presumably transported eastward by currents along the slope of the East Siberian Sea. The high chlorophyll concentration and high attenuation in this area were resulted from the high nutrient level, which was partly from rivers, and mostly from the upwelling along the slope (ACIA, 2005; Woodgate et al., 2007). The other was of Pacific origin with fewer nutrients compared to the Type-2 water, which formed Type-1 water and flowed to the northwest along the north margin of the region. Type-3 water is similar to Type-1 water and lies between Type-1 and Type-2 waters.

3.2. Vertical sections of the attenuation coefficient

Three longitudinal sections and one latitudinal section for the optical attenuation coefficient at 490 nm (Fig. 5) reveal some of the vertical features. Section 1 is the longest longitudinal section from 75°N to more than 82°N (Fig. 5a). At the ice covered region at the north, the higher attenuation coefficient was in the top 20 m coinciding with low productivity because illumination was quite limited. A very high attenuation coefficient was at 30–40 m depth over the west flank of the Mendeleev Ridge south of 78°N. For Section 2, across the Chukchi Abyssal Plain longitudinally (Fig. 5b), attenuation in the surface 30 m was very low, indicating low phytoplankton growth. The greatest attenuation occurred between 40 and 60 m, and high values were observed at the south and north ends, which belong to different water masses. To the south, the temperature at the greatest attenuation level (50 m) was -1.22 °C, consistent with shelf water formed during the winter. Attenuation coefficients and algal biomass over the shelf were much higher. The water temperature at the greatest attenuation level (48 m) at the north end was -0.47 °C, a much warmer water mass. Section 3 is a special meridional section over the narrow abyssal plain inside the Chukchi Plateau (Fig. 5c). As expected, high attenuation coefficients were observed only at Station 50, which was located far onto the shelf. The high light attenuation and high chlorophyll indicated high productivity in shelf waters. With the exception of this station, the upper ocean in this section had low attenuation of light down to 50 m. A high light

attenuation zone was observed north of 76°N at about 60 m, the deepest light attenuation zone measured during this cruise. High algal concentrations were consistent with Pacific Waters rich with nutrients in the spring, but these phytoplankton sank deeper to take advantage of available nutrients after all nutrients in the surface water were exhausted (Tremblay et al., 2008; Jiang et al., 2015). Section 4 was the only zonal section linking all three longitudinal sections (Fig. 5d). It shows light attenuation along the north margin of the observed region. The highest light attenuation zone appeared at a depth of about 40 m over the Mendeleev Ridge and the Northwind Ridge, but it was much deeper over the Chukchi Cap.

These subsurface high attenuation zones in the four sections indicate that phytoplankton blooms had occurred prior to the cruise since nutrients were exhausted in surface waters.

3.3. The integral parameters of diffuse attenuation coefficient

The spatial distribution of the attenuation coefficient can of course be integrated vertically. Here, we discuss how the attenuation depth and optical thickness are evaluated spatially.

3.3.1. Distribution of optical attenuation depth

The optical attenuation depth is defined as a depth $d(\lambda)$ at which the incident radiation is attenuated to a certain percentage, γ (Mueller et al., 2003).

$$\int_0^{d(\lambda)} k_d(z', \lambda) dz' = \ln \left[\frac{E_d(0^-, \lambda)}{E_d[d(\lambda), \lambda]} \right] = \ln \gamma. \tag{5}$$

The unit of the attenuation depth is expressed in meters. The irradiance just under the surface, $E_d(0^-, \lambda)$ is difficult to determine because of intrinsic measurement challenges, but it is replaced by γ, as $E_d[d(\lambda), \lambda] = \gamma E_d(0^-, \lambda)$. The term $d(\lambda)$ is intermediate between z_m and z_{m+1}, when the following condition is satisfied

$$\int_0^{z_m} k_d(z', \lambda) dz' \leq - \ln \gamma \leq \int_0^{z_{m+1}} k_d(z', \lambda) dz' \tag{6}$$

Here, γ was chosen to be 1% light depth for all stations to insure comparability. Based on the studies discussed in Section 3.1, the spatial difference of attenuation depths, which is spectrum dependent, was predominantly controlled by the biomass of phytoplankton in the whole water column. Here we use the attenuation depth of 490 nm as an example to illustrate regional differences (Fig. 6).
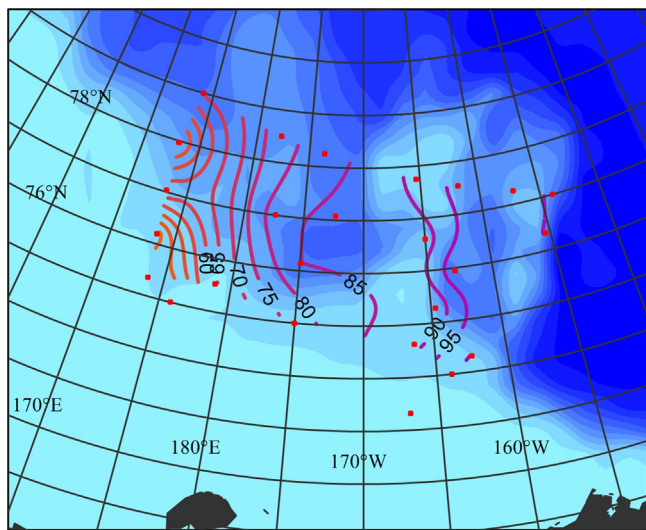
The attenuation depths are shallower to the west and deeper to the east. The deepest attenuation depth was observed at the stations adjacent to Canada Basin, at more than 100 m (Fig. 6). This indicates that in the Canada Basin the concentration of biomass was very low, maintaining maximum transparency. Based on previous work, the Chukchi Plateau and Chukchi Abyssal Plain serve as a pathway of Pacific Water in the spring (Alkire et al., 2007), and the nutrients of the Pacific-origin water were exhausted on Chukchi shelf after sea ice melt (Zhao et al., 2010). To the west, the attenuation depth is about 40 m, which means more substances were present in the water. The shallower attenuation depth is consistent with high productivity, and very high chlorophyll biomass was observed in this area. The river water discharged into the East Siberian Sea, such as Kolyma River and Indigirka River, might be a major source of nutrients that supported phytoplankton growth. In the central part of the study area over the Chikchi Abyssal Plain, attenuation depths were intermediate.

3.3.2. Distribution of the optical thickness

The optical attenuation depth is the integral attenuation property of the whole water column, while optical thickness is a
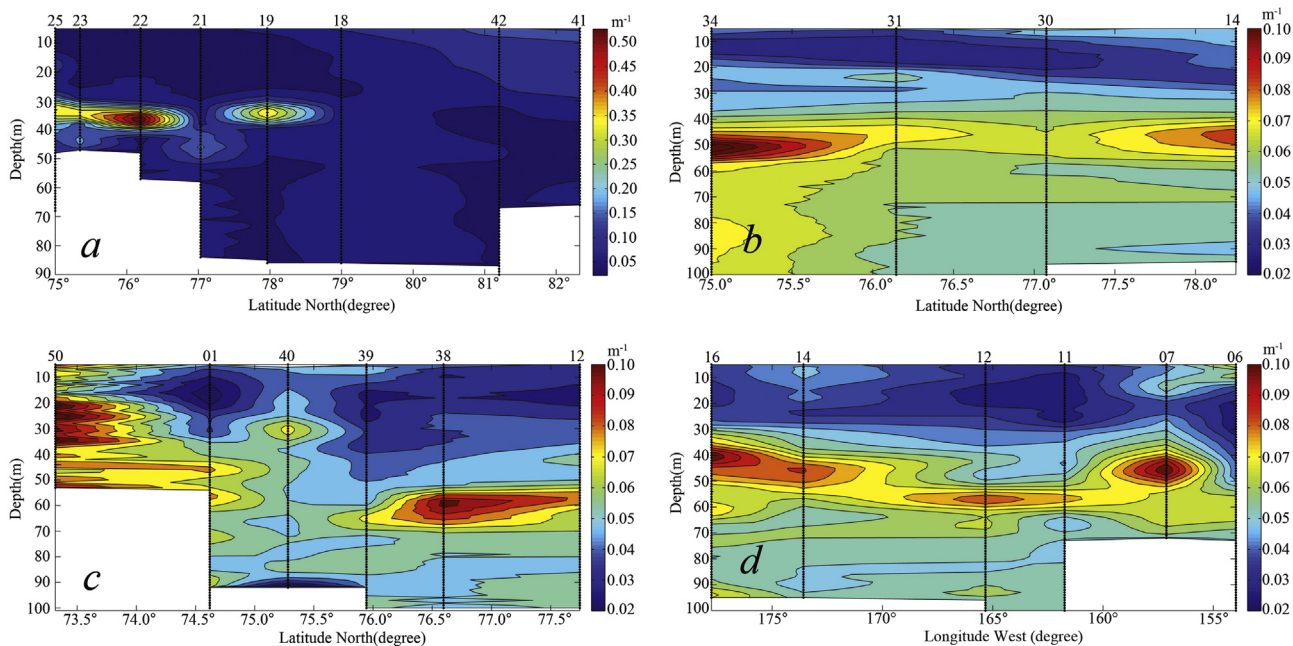
Fig. 5. Vertical distribution of the attenuation coefficient (m^{-1}) at 490 nm along four sections. Note that color scale for (b), (c) and (d) are the same, but that of (a) is scaled higher. (For interpretation of the references to color in this figure legend, the reader is referred to the web version of this article.)

Fig. 6. Spatial distribution of the attenuation depth of 490 nm (1%). The attenuation depths were shallower (< 40 m) to the west and deeper (> 100 m) to the east.

level-integrated parameter that identifies the spatial difference of attenuation. Optical thickness is defined (Mobley, 1994) using

$$\tau(\lambda) = \int_{z_1}^{z_2} c(z, \lambda)dz \qquad (7)$$

where c is the beam attenuation coefficient. The diffuse attenuation coefficient is an apparent optical property, but can also be evaluated by determining the optical thickness through reference to the definition of Eq. (7),

$$\tau(\lambda) = \int_{z_1}^{z_2} k_d(z, \lambda)dz. \qquad (8)$$

The optical thickness is therefore a non-dimensional parameter, and consists of the integration of the attenuation coefficient over a certain depth range. The integration range of optical thickness could be chosen arbitrarily to address the vertical

feature of the attenuation, but the optical thicknesses at different depths cannot be compared. However, when the optical thickness is divided by the range over which it is integrated, it is defined as the depth-averaged optical thickness (AOT), and the AOT at different depths are mutually comparable. Larger values of AOT are related to stronger attenuation.

The spatial distributions of AOT at 490 nm within each depth interval of 0–15 m, 15–30 m, 30–60 m, and 60–90 m are plotted in Fig. 7, revealing attenuation within each depth interval. For the surface 15 m, the AOT was quite small in all regions, mostly less than 0.06/m (Fig. 7a). For the most part this was consistent with low algal biomass due to limited nutrients. At depths of 15–30 m, the AOT was also very small over deep waters, but increased over the shelf, indicating high productivity at this depth (Fig. 7b). At depths of 30–60 m, a higher attenuation was observed (Fig. 7c). Nearly all the maxima for attenuation coefficients appeared at this depth interval. In deeper waters (60–90 m), the AOT declined to levels associated with surface waters (Fig. 7d).

3.4. The relationship of optical property with water mass features

A low salinity at the surface and a halocline under the mixed fresher layer were commonly seen, showing a typical seasonal halocline and high stratification. Water depths of 50 m are representative of the highest attenuation levels. At this depth, the upward heat flux is very low based upon the existence of a Near Surface Temperature Maximum (Zhao and Cao, 2011), which is nearly vertically adiabatic by strong stratification. A temperature and salinity diagram (Fig. 8) shows that at the 50 m level, temperature and salinity varied in opposite directions, with temperature higher when the salinity was lower, and vice versa. The data cluster naturally into three groups.

The warmest group (Type-1) had temperatures around 0 °C, including the stations in the Chukchi Plateau (Fig. 8), and this high temperature water at 50 m was from the Chukchi Sea. The coldest group (Type-2) had temperatures between −1.3 and −1.6 °C, and was observed at stations close to the shelf (and at two stations in the central Arctic under ice). This low temperature water originated from the continental shelf of the East Siberian Sea, where it
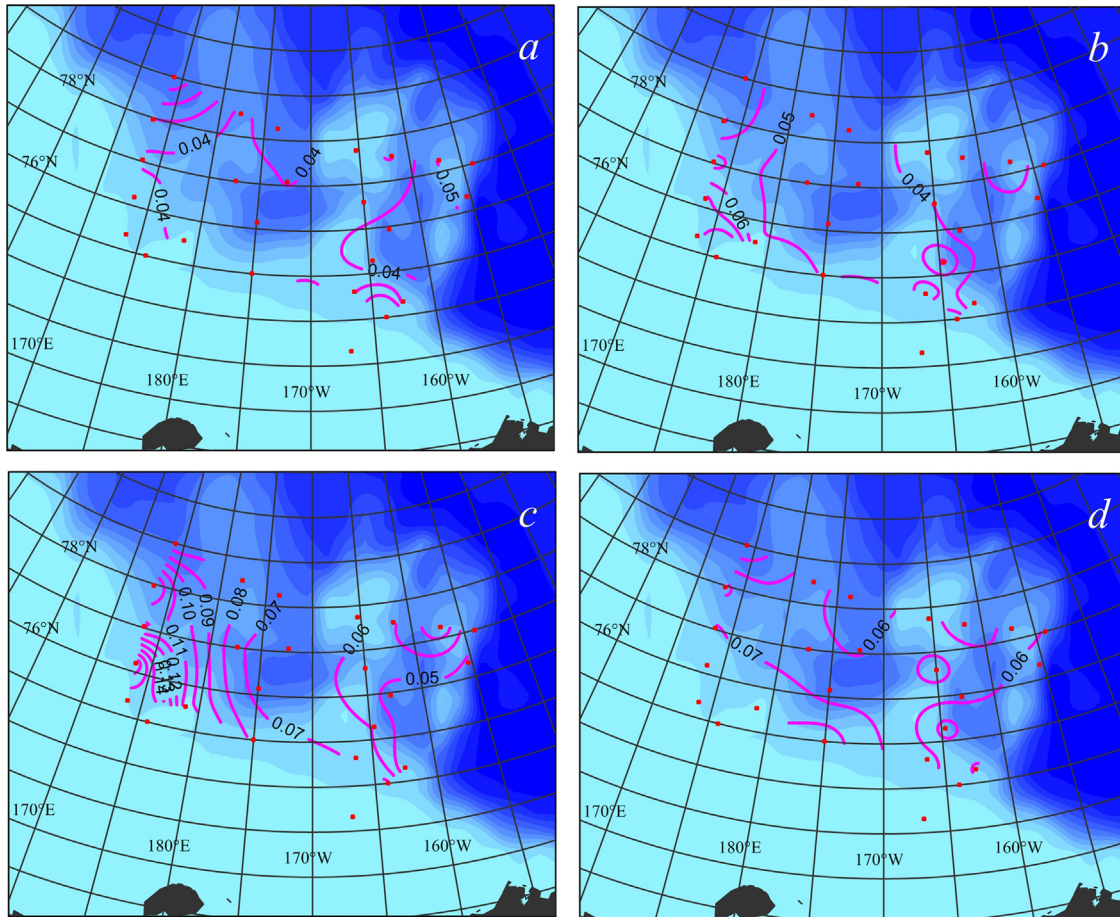
Fig. 7. Spatial distribution of average optical thickness (AOT) for 490 nm. (a) 0–15 m; (b) 15–30 m; (c) 30–60 m; (d) 60–90 m.
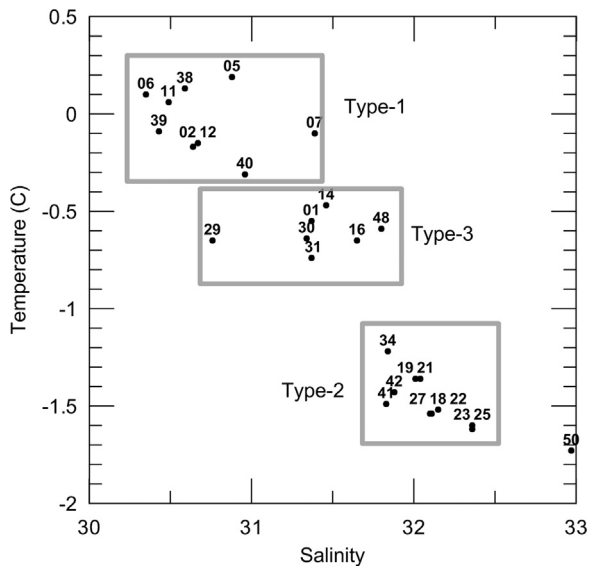

Fig. 8. Temperature and salinity diagram for water at 50 m depth. The data clustered into three groups.
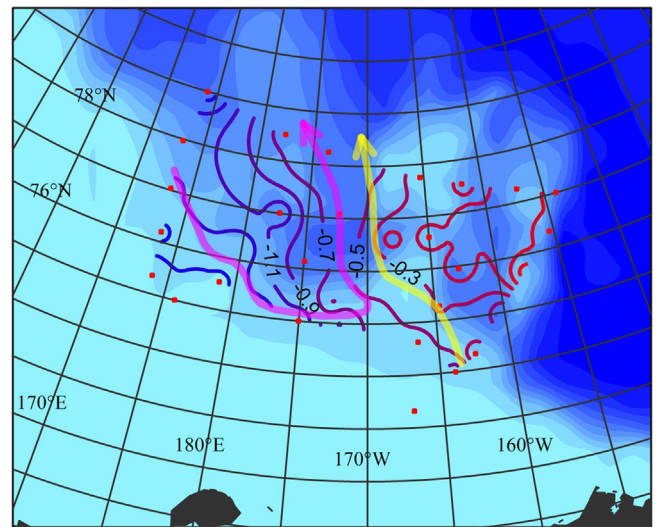

Fig. 9. Sketch of the subsurface currents. The yellow line denotes the pathway of Pacific water and the pink line denotes the flow of cold water eastly transported along the continental slope. The isotherms depict temperature at 50 m. (For interpretation of the references to color in this figure legend, the reader is referred to the web version of this article.)

was cooled by wintertime convection. We hypothesize that the cold water was transported to the east by a current along the East Siberian Sea continental slope.

An intermediate temperature group (Type-3) was observed to cluster at about −0.7 °C, including all stations over the Chukchi Abyssal Plain and Stations 01 and 48 at the continental slope area

of Chukchi Sea. We surmise that this water with moderate temperature was a mixture of warm Pacific water and cold shelf water. The temperature field at 50 m (Fig. 9) supported the possibility that the Pacific Water spread northwest over the Chukchi Plateau as denoted by the yellow line; the cold shelf

water was transported southeast along the continental slope of the East Siberian Sea, but circulated to the northwest when it encountered the Pacific Water as denoted by the pink line in Fig. 9.

The optical attenuation types were consistent with the features of water masses (Fig. 1), and were driven by biomass in the different water masses. Winter Pacific Water on the Chukchi shelf was nutrient-rich and transported to the north simultaneously with sea ice retreat (Zhao et al., 2010). The Pacific Water spread to the northwest over the Chukchi Plateau, and was transported to the Transpolar Drift based on the previous study and was consistent with the optical properties of Type-1 water. Shelf water transported eastward along the continental slope was not only consistent with observed temperatures (Fig. 9), but also by the optical features of Type-2 waters. Pacific Winter Water carries nutrients into the northern Chukchi Sea that stimulates production in spring. However, the high attenuation coefficient of Type-2 water indicated that productivity along the continental slope was much higher than that associated with Pacific Water, which is a notable phenomenon. A possible recirculation might exist over the Chukchi Abyssal Plain (pink line, Fig. 9), as the eastward current along the slope was blocked by the warm Pacific Water. The optical data also supported the existence of recirculation. Over the Chukchi Abyssal Plain, water optical features were Type-3, which was sandwiched between Type-2 water to the south and west, and Type-1 water to the north and east. The recirculated water was well mixed with Pacific Water, thus increasing its temperature.

The flow over the Chukchi Plateau to the northwest is easy to understand. It is driven by the sea level difference between Pacific and Atlantic oceans, and enhanced by the wind field of Beaufort High (Stigebrandt, 1984). However, the eastward flow along the continental slope of the East Siberian Sea shown by the pink line in Fig. 9 cannot be understood by a geostrophic current, as there is no a mechanism to build a high pressure on the shelf. The subsurface current, along with the underlying boundary current, do not match the isobaths of dynamic height, because they are compensation currents. These eastward currents along the slope could be driven by following mechanism: the volume flux of the Transpolar Drift is larger than the flux through the Bering Strait, and produces near surface volume loss; the slope current is part of the compensation movement to supply the Transpolar Drift. Aagaard (1981) suggested the possibility that cooling and freshening of Atlantic waters could upwell onto the Chukchi shelf. Woodgate et al., (2005) further indicated that much of the western Arctic's lower halocline was influenced by a diapycnal mixing of Pacific winter waters and Atlantic origin water over the northern Chukchi shelf/slope. The surface current responds the wind driven, which usually induces a westward current (Lukovich and Barber, 2006), but it benefits to produce a compensation current and an upwelling along the slope.

4. Discussion and conclusion

Irradiance measurement data during Korean 2012 summer cruise are used to study the optic properties over the Mendeleev Ridge, Chukchi Abyssal Plain, and Chukchi Plateau area.

Attenuation properties at all stations can be sorted into three types based on the attenuation coefficient of 490 nm. Most of the observed optical properties belonged to Types 1, 2, and 3. Type-2 water had a maximum attenuation coefficient of up to 0.56/m located over the west flank of the Mendeleev Ridge and continental slope. Type-1 was similar to Type-2, but with a weaker maximum attenuation coefficient of less than 0.1/m located at the north margin of the observed region. The attenuation coefficients in Type-3 water were the lowest of all of types observed.

The most reasonable explanation for the intense maximum of the attenuation coefficient in Type-2 water is the nutrient-rich water in the upper ocean in spring. When nutrients in the surface layers became exhausted, the algae had sank to deeper levels for utilizing nutrient. Although the water underneath was nutrient-rich, illumination was very low. The resulting biomass was best understood as a result of optimization between sufficient nutrients and illumination.

The difference between Type-1 and Type-2 waters suggested that there were essentially two surface water masses in the observed region. One was shelf water that was well-mixed with river water, which was transported to the east by a current along the East Siberian Slope. The other was the water from Pacific with lower nutrient concentration and transported to the northwest along the north margin of the observed region.

The attenuation coefficient in all surface levels with exception of the shelf stations was low because nutrients at the surface had become exhausted. The attenuation depth was shallower to the west ($\sim$40 m) and deeper to the east. The deepest attenuation depth was at the stations within the Canada Basin, and was at more than 100 m. The averaged optical thickness was also studied in this work to identify the gradients of attenuation. Depths of 30–60 m were the main depths with observed high attenuation.

We confirmed that optical attenuation was related to the water mass features. Cold water temperatures ($-1.4\ °C$) were consistent with Type-2 water, which was transported by the slope current to the east. Higher water temperatures (around $0\ °C$) were observed over the Chukchi Plateau, coming from the Pacific through the Chukchi Sea. An intermediate temperature region about $-0.7\ °C$ was observed over the Chukchi Abyssal Plain, which may be a recirculated branch of shelf water, mixed with Pacific Water.

Acknowledgements

References

Alkire, M.B., Falkner, K., Rigor, K., Steele, I.M, Morison, J., 2007. The return of Pacific waters to the upper layers of the central Arctic Ocean. Deep Sea Res. Part I 54 (9), 1509–1529.

Aagaard, K., 1981. On the deep circulation in the Arctic Ocean. Deep-Sea Res. 28, 251–268.

Arctic Climate Impact Assessment, 2005. Arctic Climate Impact Assessment. Scientific Report. Cambridge University Press, Cambridge, U.K..

Chang, G.C., Dickey, T.D., 2004. Coastal ocean optical influences on solar transmission and radiant heating rate. J. Geophys. Res. 109, C01020. http://dx.doi.org/10.1029/2003JC001821.

Dickey, T.D., 1991. The emergence of concurrent high-resolution physical and bio-optical measurements in the upper ocean and their applications. Rev. Geophys. 29 (3), 383–413.

Dickey, T., Lewis, M., Chang, G., 2006. Optical oceanography: recent advances and future directions using global remote sensing and in situ observations. Rev. Geophys. 44, 1–39.

Gordeev, V.V., 2006. Fluvial sediment flux to the Arctic Ocean. Geomorphology 80, 94–104.

Gordeev, V.V., Martin, J.-M., Sidorov, I.S., Sidorova, M.N., 1996. A reassessment of the Eurasian water, sediment, major ions, and nutrients to the Arctic Ocean. Am. J. Sci. 296, 664–691.

Gordon, H.R., 1991. Absorption and scattering estimates from irradiance measurements: Monte Carlo simulations. Limnol. Oceanogr. 36, 769–777.

Hill, V., Cota, G., 2005. Spatial patterns of primary production on the shelf, slope and basin of the western Arctic in 2002. Deep Sea Res. Part II 52, 3344–3354. http://dx.doi.org/10.1016/j.dsr2.2005.10.001.

Jahn, A., Tremblay, L.B., Newton, R., Holland, M.M., Mysak, L.A., Dmitrenko, I.A., 2010. A tracer study of the Arctic Ocean's liquid freshwater export variability. J. Geophys. Res. 115, C07015. http://dx.doi.org/10.1029/2009JC005873.

Jerlov, N.G., 1976. Marine Optics, Elsevier Oceanography Series, vol. 14. Elsevier, New York p. 231.

Jiang, Y., Yang, E.J., Min, J.O., Kim, T.W., Kang, S.H., 2015. Vertical variation in the ecological characteristics of pelagic ciliate communities in the western Arctic Ocean. Deep Sea Res. 120, 103–113. http://dx.doi.org/10.1016/j.dsr2.2014.09.005.

Jones, E.P., Anderson, L.G., Swift, J.H., 1998. Distribution of Atlantic and Pacific waters in the upper Arctic Ocean: implications for circulation. Geophys. Res. Lett. 25 (6), 765–768.

Lindsay, R.W., Zhang, J., 2005. The thinning of Arctic sea ice, 1988–2003: have we passed a tipping point? J. Clim. 18 (22), 4879–4894.

Lukovich, J.V., Barber, D.G., 2006. Atmospheric controls on sea ice motion in the southern Beaufort Sea. J. Geophys. Res. 111 (D18103), http://dx.doi.org/10.1029/2005JD006408.

Manizza, M., Le Que´re´, C., Watson, A.J., Buitenhuis, E.T., 2005. Bio-optical feedbacks among phytoplankton, upper ocean physics and sea-ice in a global model. Geophys. Res. Lett. 32, L05603. http://dx.doi.org/10.1029/2004GL020778.

Matsuoka, A., Larouche, P., Poulin, M., Vincent, W., Hattorie, H., 2009. Phytoplankton community adaptation to changing light levels in the southern Beaufort Sea, Canadian Arctic. Estuar., Coast. Shelf Sci. 82, 537–546.

Mitchell, B.G., Holm-Hansen, O., 1991. Observations and modeling of the Antarctic phytoplankton crop in relation to mixing depth. Deep-Sea Res. 38 (8/9), 981–1007.

Mitchell, B.G., 1992. Predictive bio-optical relationships for polar oceans and marginal ice zones. J. Mar. Syst. 3, 91–105.

Mobley, C.D., 1994. Light and Water; Radiative Transfer in Natural Waters. Academic Press, San Diego p. 592.

Morel, A., 1988. Optical modelling of the upper ocean in relation to its biogenous matter content (case I waters). J. Geophys. Res. 93, 10,749–10,768.

Morel, A., Maritorena, S., 2001. Bio-optical properties of oceanic waters: a reappraisal. J. Geophys. Res. 106 (C4), 7163–7180.

Mueller, J.L., Fargion, G.S., McClain, C.R., 2003. Ocean Optics Protocols For Satellite Ocean Color Sensor Validation. Revision 5, Vol. V: Biogeochemical and Bio-Optical Measurements and Data Analysis Protocols. NASA Goddard Space Flight Center, MD.

Mueller, J.L., Fargion, G.S., 2003. Ocean Optics Protocols for SeaWiFS Validation, Revision 4. NASA/TM-2003-21621. NASA Goddard Space flight center, Greenbelt, Maryland p. 308.

Nakamoto, S., Kumar, S.P., Oberhuber, J.M., Ishizaka, J., Muneyama, K., Frouin, R., 2000. Response of the equatorial Pacific to chlorophyll pigment in a mixed layer isopycnal ocean general circulation model. Geophys. Res. Lett. 28, 2021–2024.

Nishino, S., Shimada, K., Itoh, M., Yamamoto-Kawai, M., Chiba, S., 2008. East–west differences in water mass, nutrient, and chlorophyll a distributions in the sea ice reduction region of the western Arctic Ocean. J. Geophys. Res. 113, C00A01. http://dx.doi.org/10.1029/2007JC004666.

Pabi, S., van Dijken, G.L., Arrigo, K.R., 2008. Primary production in the Arctic Ocean, 1998–2006. J. Geophys. Res. 113, C08005. http://dx.doi.org/10.1029/2007JC004578.

Pegau, W.S., 2002. Inherent optical properties of the central Arctic surface waters. J. Geophys. Res. 107 (C10), 8035. http://dx.doi.org/10.1029/2000JC000382.

Perovich, D.K., Light, B., Eicken, H., Jones, K.F., Runciman, K., Nghiem, S.V., 2007. Increasing solar heating of the Arctic Ocean and adjacent seas, 1979–2005: Attribution and role in the ice-albedo feedback. Geophys. Res. Lett. 34, L19505. http://dx.doi.org/10.1029/2007GL031480.

Perovich, D.K., Richter-Menge, J.A.K., Jones, F., Light, B., 2008. Sunlight, water, and ice: Extreme Arctic sea ice melt during the summer of 2007. Geophys. Res. Lett. 35, L11501. http://dx.doi.org/10.1029/2008GL034007.

Perovich, D.K., Richter-Menge, J.A., 2009. Loss of Sea Ice in the Arctic. Annu. Rev. Mar. Sci. 1, 417–441.

Perrette, M., Yool, A., Quartly, G.D., Popova, E.E., 2011. Near-ubiquity of ice-edge blooms in the Arctic. Biogeosciences 8, 515–524. http://dx.doi.org/10.5194/bg-8-515-2011.

Popova, E.E., Yool, A., Coward, A.C., Aksenov, Y.K., Alderson, S.G., de Cuevas, B.A., Anderson, T.R., 2010. Control of primary production in the Arctic by nutrients and light: insights from a high resolution ocean general circulation model. Biogeosciences 7, 3569–3591. http://dx.doi.org/10.5194/bg-7-3569-2010.

Sakshaug, E., 2003. Primary and secondary production in the Arctic Seas. In: Stein, R., Macdonald, R.W. (Eds.), The Organic Carbon Cycle in the Arctic Ocean. Springer-Verlag, Berlin, pp. 57–81.

Sathyendranath, S., Gouveia, A.D., Shetye, A.R., Ravindran, P., Platt, T., 1991. Biological control of surface temperature in the Arabian Sea. Nature 349, 54–56.

Sathyendranath, S., Stuart, V., Cota, G., Maas, H., Platt, T., 2001. Remote sensing of phytoplankton pigments: a comparison of empirical and theoretical approaches. Int. J. Remote Sens. 22, 249–273.

Schlosser, P., Newton, B., Ekwurzel, B., Khatiwala, S., Mortlock, R., Fairbanks, R., 2002. Decrease of river runoff in the upper waters of the Eurasian Basin, Arctic Ocean, between 1991 and 1996: Evidence from $\delta^{18}O$ data. Geophys. Res. Lett. 29 (9), 1289. http://dx.doi.org/10.1029/2001GL013135.

Shell, K.M., Frouin, R., Nakamoto, S., Somerville, R.C.J., 2003. Atmospheric response to solar radiation absorbed by phytoplankton. J. Geophys. Res. 108 (D15), 4445. http://dx.doi.org/10.1029/2003JD003440.

Shimada, K., Carmack, E.C., Hatakeyama, K, Takizawa, T., 2001. Varieties of shallow temperature maximum waters in the Western Canadian basin of the Arctic Ocean. Geophys. Res. Lett. 28 (18), 3441–3444.

Shimada, K., Kamoshida, T., Itoh, M., Nishino, S., Carmack, E., McLaughlin, F.A., Zimmermann, S., Proshutinsky, A., 2006. Pacific Ocean inflow: influence on catastrophic reduction of sea ice cover in the Arctic Ocean. Geophys. Res. Lett. 33, L08605. http://dx.doi.org/10.1029/2005GL025624.

Siegel, D.A., Ohlmann, J.C., Washburn, L., Bidigare, R., Nosse, C.T., Fields, E., Zhou, Y., 1995. Solar radiation, phytoplankton pigments and the radiant heating of the equatorial warm pool. J. Geophys. Res. 100, 4885–4891.

Smith, R.C., Baker, K.S., 1984. Analysis of ocean optical data, Ocean Optics VII. In: Blizard, M. (Ed.), SPIE, 478; 1984, pp. 119–126.

Smith, R.C., Bake,r, K.S., 1986. Analysis of ocean optical data, Ocean Optics VIII. In: Slater, P.N. (Ed.), SPIE, 637; 1986, pp. 95–107.

Steele, M., Morison, J., Ermold, W., Rigor, I., Ortmeyer, M., Shimada, K., 2004. Circulation of summer Pacific halocline water in the Arctic Ocean. J. Geophys. Res. 109 (C02027), http://dx.doi.org/10.1029/2003JC002009.

Stigebrandt, A., 1984. The North Pacific: a global scale estuary. J. Phys. Oceanogr. 14, 464–470.

Stroeve, J., Serezze, M., Drobot, S., Gearheard, S., Holland, M., Maslanik, J., Meier, W., Scambos, T., 2008. Arctic sea ice plummets in 2007. Eos Trans. AGU 89, 13.

Strutton, P.G., Chavez, F.P., 2004. Biological heating in the equatorial pacific: Observed variability and potential for real-time calculation. J. Clim. 17, 1097–1109.

Tremblay, J.É., Simpson, K., Martin, J., Miller, L., Gratton, Y., Barber, D., Price, N.M., 2008. Vertical stability and the annual dynamics of nutrients and chlorophyll fluorescence in the coastal, southeast Beaufort Sea. J. Geophys. Res. Oceans 113, C07S90. http://dx.doi.org/10.1029/2007JC004547.

Tucker III, W.B., Weatherly, J.W., Eppler, D.T., Farmer, L.D., Bentley, D.L., 2001. Evidence for rapid thinning of sea ice in the western Arctic Ocean at the end of the 1980s. Geophys. Res. Lett. 28, 2851–2854.

Wegner, C., Hölemann, J.A., Dmitrenko, I., Kirillov, S., Tuschling, K., Abramova, E., Kassens, H., 2003. Suspended particulate matter on the Laptev Sea shelf (Siberian Arctic) during ice-free conditions. Estuar., Coast. Shelf Sci. 57 (1/2), 55–64.

Woodgate, R.A., Aagaard, K., Swift, J.H., Falkner, K.K., Smethie Jr., W.M., 2005. Pacific ventilation of the Arctic Ocean's lower halocline by upwelling and diapycnal mixing over the continental margin. Geophys. Res. Lett. 32, L18609. http://dx.doi.org/10.1029/2005GL023999.

Woodgate, R.A., Aagaard, K., Swift, J.H., Smethie Jr., W.M., Falkner, K.K., 2007. Atlantic water circulation over the Mendeleev Ridge and Chukchi Borderland from thermohaline intrusions and water mass properties. J. Geophys. Res. 112, C02005. http://dx.doi.org/10.1029/2005JC003416.

Wozniak, B., Dera, J., 2007. Light Absorption in Sea Water. Springer Sciences+Business Media. LLC, New York p. 454.

Yentsch, C.S., Phinney, D.A., 1989. A bridge between ocean optics and microbial ecology. Limnol. Oceanogr. 34, 1694–1705.

Zhao, J.-P., Cao, Y., 2011. Summer water temperature structures in upper Canada Basin and their interannual variation. Adv. Polar Sci. 22 (4), 223–234.

Zhao, J.-P., Shi, J.-X., Jin, M.-M., Gao, G.-P., Jiao, Y.-T., Lu, Y., 2010. The water structure of Chukchi Sea during the ice melting process. Adv. Geosci. 25 (2), 154–162 (In Chinese with English Abstract).